Available online at www.sciencedirect.com
ScienceDirect
Journal of the European Ceramic Society 27 (2007) 4759–4765
www.elsevier.com/locate/jeurceramsoc

Processing of hot pressed Al_2O_3–Cr_2O_3/Cr-carbide nanocomposite prepared by MOCVD in fluidized bed

Hao-Tung Lin [a], Sheng-Chang Wang [b], Jow-Lay Huang [a,*], Shin-Yun Chang [a]

[a] *Department of Materials Science and Engineering, National Cheng-Kung University, Tainan 701, Taiwan, ROC*
[b] *Department of Mechanical Engineering, Southern Taiwan University of Technology, Tainan 710, Taiwan, ROC*

Received 27 September 2006; received in revised form 12 February 2007; accepted 18 February 2007
Available online 24 April 2007

Abstract

Nanosized particles dispersed uniformly on Al_2O_3 particles were prepared from the decomposition of precursor $Cr(CO)_6$ by metal organic chemical vapor deposition (MOCVD) in a fluidized chamber. These nanosized particles consisted of Cr_2O_3, CrC_{1-x}, and C. A solid solution of Al_2O_3–Cr_2O_3 and an Al_2O_3–Cr_2O_3/Cr_3C_2 nanocomposite were formed when these fluidized powders were pre-sintered at 1000 and 1150 °C before hot-pressing at 1400 °C, respectively. In addition, an Al_2O_3–Cr_2O_3/Cr-carbide (Cr_3C_2 and Cr_7C_3) nanocomposite was formed when the particles were directly hot pressed at 1400 °C. The interface between Cr_3C_2 and Al_2O_3 is non-coherent, while the interface between Cr_7C_3 and Al_2O_3 is semi-coherent.

Keywords: Precursors-organic; Composites; Interfaces; Al_2O_3; Cr_2O_3

1. Introduction

Alumina has been much used in structural ceramic applications because of its excellent mechanical properties, good chemical stability, and high temperature characteristics. Various second phase particles have been reported in the literature as additives to improve its inherent brittle property.[1–3] A composite consisting of Al_2O_3 as a matrix and micro-sized Cr_3C_2 as the second phase reinforcing particle has been prepared by Huang,[4–6] Fu and coworkers.[7,8] These Al_2O_3/Cr_3C_2 composites demonstrated superior mechanical properties to those of the matrix phase due to the high Young's modulus of Cr_3C_2 and its outstanding ability to resist high-temperature erosion at temperatures up to 1000 °C.[9] In addition, the good electrical conductivity of Cr_3C_2[10] makes electrical discharge machining possible.

Besides second phase particles, solid solution strengthening is another mechanism for the Al_2O_3 matrix. Chromia (Cr_2O_3) has been used to improve the physical properties of Al_2O_3.[11–14] As Cr_2O_3 has the same corundum crystal structure as Al_2O_3, Al_2O_3–Cr_2O_3 can form substitutional solid solution in all ranges at high temperature. The addition of Cr_2O_3 was found to increase the hardness, tensile strength, and thermal shock resistance of Al_2O_3.

More attention has been given to nanocomposites since Niihara et al.[15] reported that advantages of nanometer inclusions are able to achieve several benefits. The nanometer inclusions are difficult to be uniformly dispersed within the microscaled matrix particles. This problem arises since that the nanosized particles are easy to agglomerate due to the interaction between the particles. The agglomerate will promote the generation of voids during densification and produce microstructural non-homogeneity.[16] It has been found that the combination of conventional fluidized bed technology with CVD is an effective method to deposit particles on powders.[17–19] The advantage of this method is that a fluidized bed provides uniform temperature and concentration of decomposed precursor to make the good dispersion of fine particles on the fluidized particles.[20]

In this present work, nanometer-sized Cr_2O_3 coated on micrometer-sized Al_2O_3 has been prepared by MOCVD in a fluidizing reactor, using $Cr(CO)_6$ as the precursor. An Al_2O_3-based nanocomposite containing nanosized Cr-carbide particles (Cr_3C_2, Cr_7C_3) and solid solution Al_2O_3–Cr_2O_3 can be hot pressed. The processing and microstructure development of these nanocomposites are particularly discussed here. The mechanical properties of these nanocomposites will be the subject for further publications.

* Corresponding author. Tel.: +886 6 234 8188; fax: +886 6 276 3586.
E-mail address: JLH888@mail.ncku.edu.tw (J.-L. Huang).

0955-2219/$ – see front matter © 2007 Elsevier Ltd. All rights reserved.
doi:10.1016/j.jeurceramsoc.2007.02.207

Table 1
Sintering conditions of samples

Samples	Sintering powders	Sintering conditions
ALO	Pure alumina powder	1400 °C/1 h, pressure 25 MPa
Sample 1	Composite powders fluidized at 300 °C for 1 h	1000 °C/1 h, then 1400 °C/1 h, pressure 25 MPa
Sample 2	Composite powders fluidized at 300 °C for 1 h	1150 °C/1 h, then 1400 °C/1 h, pressure 25 MPa
Sample 3	Composite powders fluidized at 300 °C for 1 h	1400 °C/1 h, pressure 25 MPa

2. Experiment

2.1. Powder and sample preparation

Chromium hexacarbonyl ($Cr(CO)_6$, 99%, Strem Chemicals Co., USA) was used as the precursor of chromium oxide in the MOCVD process. Aluminum oxide powder (A16SG, Alcoa, USA) was used as the matrix powder, and the average particle size was about 0.2–0.4 μm. A vaporized precursor carried by He gas (99.9% pure) was introduced into the fluidized bed reactor for the MOCVD process. Based on Lander's results,[21] the precursor container was kept at 75 °C in a vacuum (10 torr) in the present experiment. The $Cr(CO)_6$ vapor was decomposed in the fluidized chamber at 300 °C, causing it to leave a deposit on the fluidizing alumina particles in the chamber. A detailed description of the process can be found elsewhere.[22]

2.2. Densification

The 200 mesh fluidized powder is first die-pressed, and then put into a BN-coated graphite die and hot-pressed at a pressure of 25 MPa in a HP furnace (High-multi 5000, Fujidempa Kogyo Co., Ltd., Japan) at 1400 °C under vacuum (5×10^{-4} torr). The detailed sintering conditions of the different samples are listed in Table 1.

2.3. Characterization of properties

The deposited particles and hot pressed pieces were analyzed by XRD (Rigaku D/MaxIII, Japan) using Cu K radiation of 1.5418 Å wavelength. FEG-TEM (field emission gun transmission electron microscopy, FEI Tecnal F20, USA) equipped with high angle annular dark field (HAADF) scanning transmission electron microscopy (STEM) was used to characterize the phase composition and microstructure. In addition, XPS (X-ray photoelectron spectroscopy, VG Scientific 210, England) was used to identify the coating phases by their binding energy. An image analysis program of Matrox Inspector 2.2 was utilized to determine the matrix grain size and volume percents of the reinforcing particles based on the micrographs.

3. Results and discussion

3.1. Characteristics of particles prepared by the pyrolysis of $Cr(CO)_6$

The vaporized precursor $Cr(CO)_6$ decomposed at 300 °C in the reaction chamber without alumina powder as the matrix. Fig. 1(a) shows the TEM micrograph of the particles of decom-

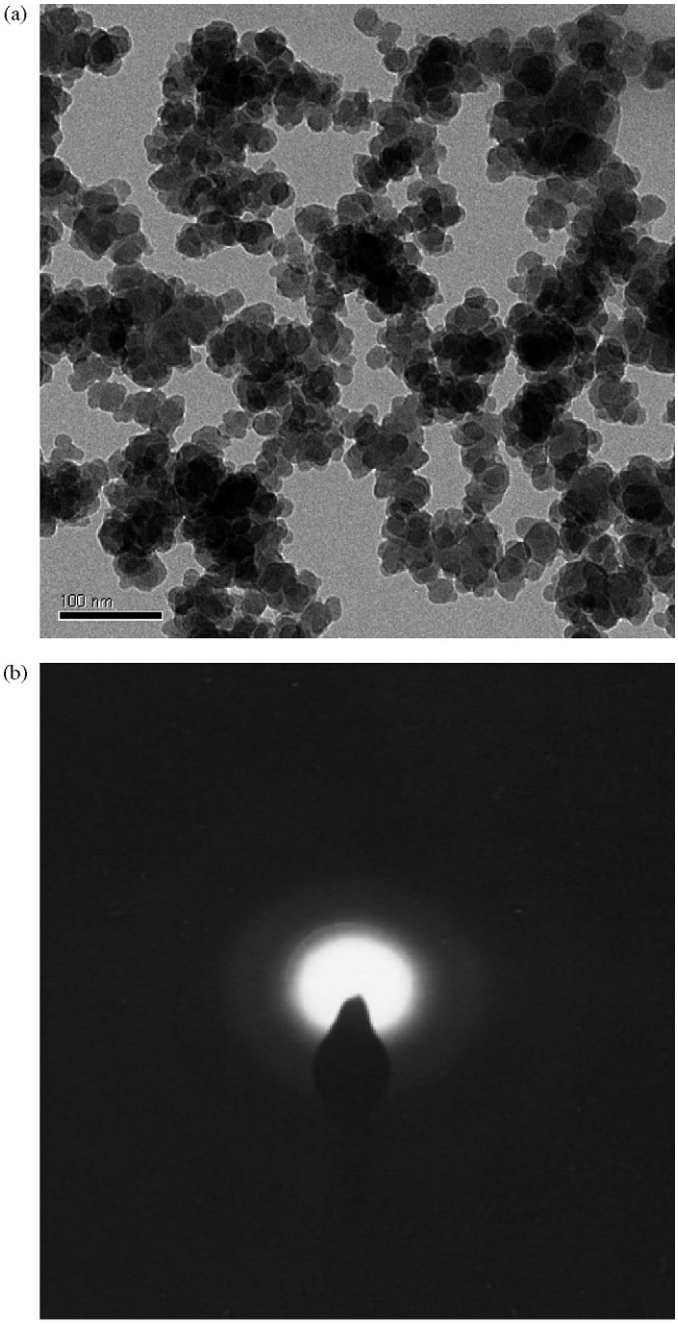

Fig. 1. (a) TEM micrograph of nanosized particles of decomposed $Cr(CO)_6$ prepared at 300 °C. (b) TEM diffraction pattern shows the nanosized particle is an amorphous phase.

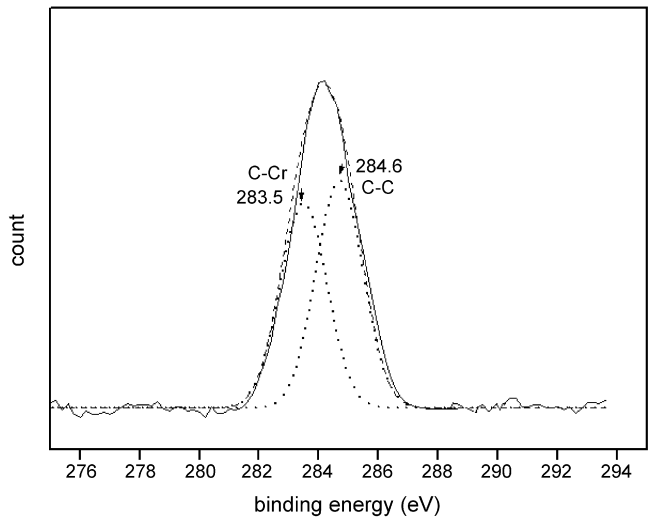

Fig. 2. X-ray photoelectron spectra of the C1s regions of decomposed $Cr(CO)_6$ prepared at 300 °C in fluidized bed.

posed $Cr(CO)_6$ collected from the fluidized chamber wall. It can clearly be observed that the particles are nanosized. Fig. 1(b) shows the TEM electron diffraction pattern of the nanosized particles in Fig. 1(a). It demonstrates that the particles of decomposed $Cr(CO)_6$ are amorphous. The XPS spectra of the particles of decomposed $Cr(CO)_6$, with bonding energy at the C1s and Cr2p regions, are displayed in Figs. 2 and 3, respectively. In Fig. 2, the solid line is the experimental data, the dashed line is used to fit the data, and the dotted lines are deconvolutions of the fit into two peaks. The XPS spectra of the C1s regions in Fig. 2 provide evidence that at least two forms of carbon bonding exist in the particles of decomposed $Cr(CO)_6$. One is carbon bonded to chromium atoms (C–Cr) at 283.5 eV, and the other is free carbon (C–C) at 284.6 eV. Fig. 3 indicates two peaks corresponding to the spin-orbit splitting $2p_{1/2}$ and $2p_{3/2}$ of Cr, which has a bonding energy of 586.3 and 576.6 eV, respectively. The band shift of these two peaks is 9.7 eV, which indicates the existence of Cr_2O_3

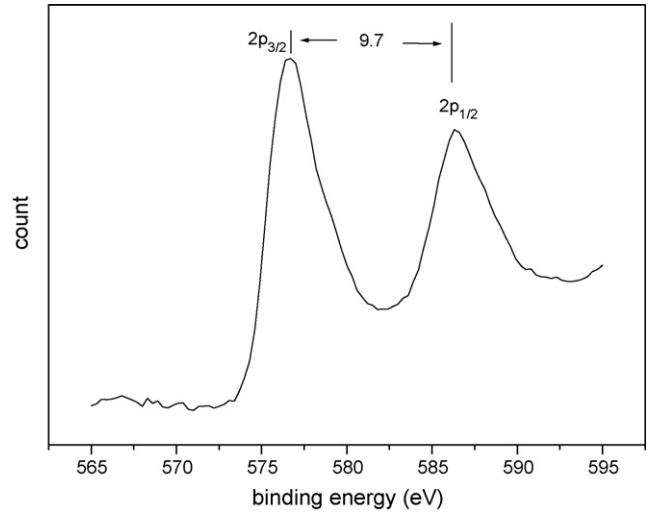

Fig. 3. X-ray photoelectron spectra of the Cr 2p regions of decomposed $Cr(CO)_6$ prepared at 300 °C in fluidized bed.

in the particles of decomposed $Cr(CO)_6$.[23] During pyrolysis, the CO ligands in $Cr(CO)_6$ gradually disappeared[24] and produced Cr and CO. However, Shinn and his collaborators[25] report that the CO molecules are unstable and have a tendency to chemisorb onto the surface of transition metals, causing the bond between carbon and oxygen to break after the occurance of chemisorption. Therefore, the XPS results showing that the products of the decomposed $Cr(CO)_6$ are Cr_2O_3, carbide (Cr–C) and free carbon are reasonable. Schuste et al.[26] report that CrC_{1-x} and free carbon are fabricated in the coating when $Cr(CO)_6$ is used as the precursor in the MOCVD process. In our study, the carbide CrC_{1-x}, corresponding to the C–Cr binding in the XPS in Fig. 2, was found in the particles of decomposed $Cr(CO)_6$. Bouzy and coworkers[27] found C atoms in the octahedral interstitial sites of the cubic-closed Cr packing in the non-stoichiometric CrC_{1-x} structure.

3.2. Characteristics of nano-particles deposited on the alumina

Fig. 4 shows the TEM micrograph of the fluidized particles; it clearly shows that the nanosized Cr-species particles are well dispersed on the surfaces of the alumina when the alumina powders have been used as the matrix powder in the fluidized chamber at 300 °C for 2 h. This result indicates that the vaporized $Cr(CO)_6$ precursor can be deposited on the surfaces of fluidizing alumina particles via the pyrolysis effect by means of a combination of chemical vaporized deposition and fluidized bed technique.

Fig. 5 shows the XRD patterns of the fluidizing powders treated at a variety of temperatures from 700 to 1150 °C in the graphite furnace in a vacuum for 2 h. The Cr_2O_3 peaks seen in the XRD patterns clearly indicate that the amorphous

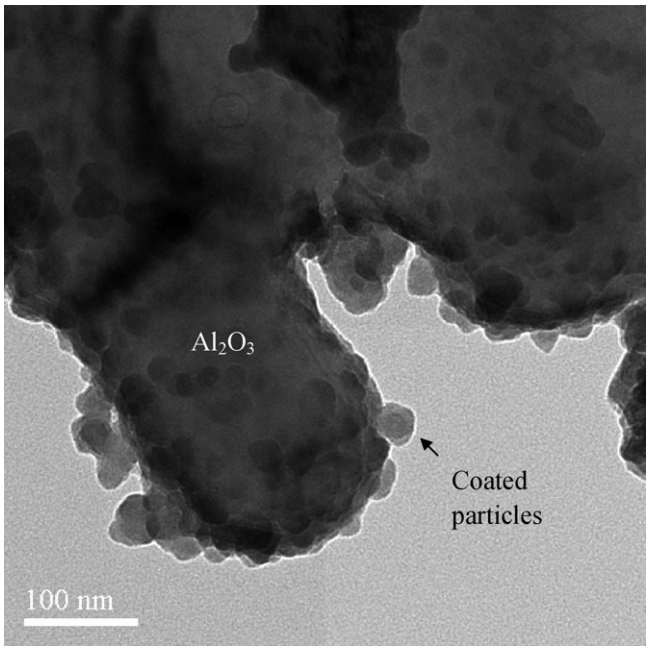

Fig. 4. TEM micrograph of nano-particles deposited on the surface of Al_2O_3 particles.

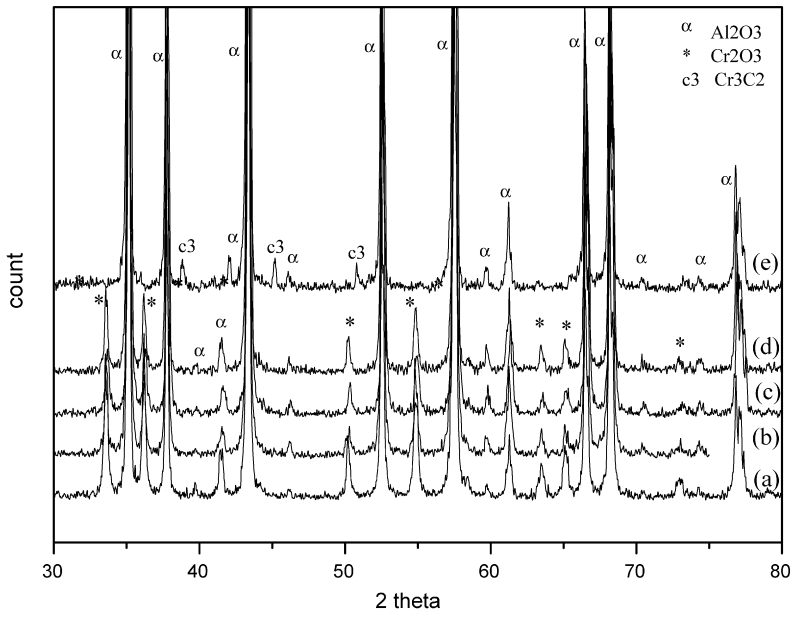

Fig. 5. XRD patterns of the powder thermally treated at a variety of temperatures: (a) 700 °C, (b) 800 °C, (c) 900 °C, (d) 1000 °C, and (e) 1150 °C in a vacuum in a graphite furnace for 2 h for the fluidized powders prepared in the fluidized bed.

Cr_2O_3 has crystallized, but does not carbonize at temperatures under 1000 °C. As, Bouzy[27] and Bewilogua[28] report, an annealing treatment causes a transformation of the metastable carbide CrC_{1-x} into the stable carbide phase Cr_3C_2. In this study, Cr_3C_2 peaks are not observed in the XRD patterns shown in Fig. 5(a)–(d), consequently, suggesting that the CrC_{1-x} content of the decomposed $Cr(CO)_6$ is too little to be found in XRD patterns. According to the XRD pattern shown in Fig. 5(e), Cr_2O_3 reacts with carbon and transforms into Cr_3C_2 when the treatment temperature is 1150 °C. This carbothermal reaction process[9] can be shown as reaction (1):

$$Cr_2O_{3(s)} + 13/3C_{(s)} \rightarrow 2/3Cr_3C_{2(s)} + 3CO_{(g)} \quad (1)$$

3.3. The formations of Cr-carbide/Al_2O_3 nanocomposite and Cr_2O_3/Al_2O_3 solid solution

The detailed sintering conditions of the different samples of ALO, sample 1, sample 2, and sample 3, are shown in Table 1. Fig. 6 shows the XRD patterns of the samples thermally treated under different conditions. The Si peaks shown in the XRD pattern were used for calibration.

First, Fig. 6(a) and (b) indicate that the Al_2O_3 peaks for sample 1 shifted to lower angles than those for ALO. With ALO the pure alumina powder was hot pressed at 1400 °C, while with sample 1 the fluidized powder was pre-sintered at 1000 °C before the hot pressing at 1400 °C. During the pre-sintering at 1000 °C, most of the Cr_2O_3 reacted with Al_2O_3 to form an Al_2O_3–Cr_2O_3

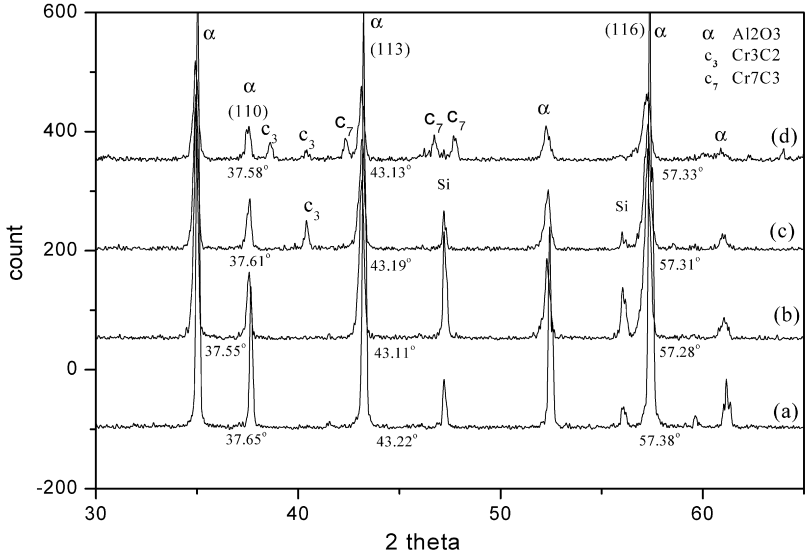

Fig. 6. XRD patterns of hot pressed samples: (a) ALO, (b) sample 1, (c) sample 2, and (d) sample 3.

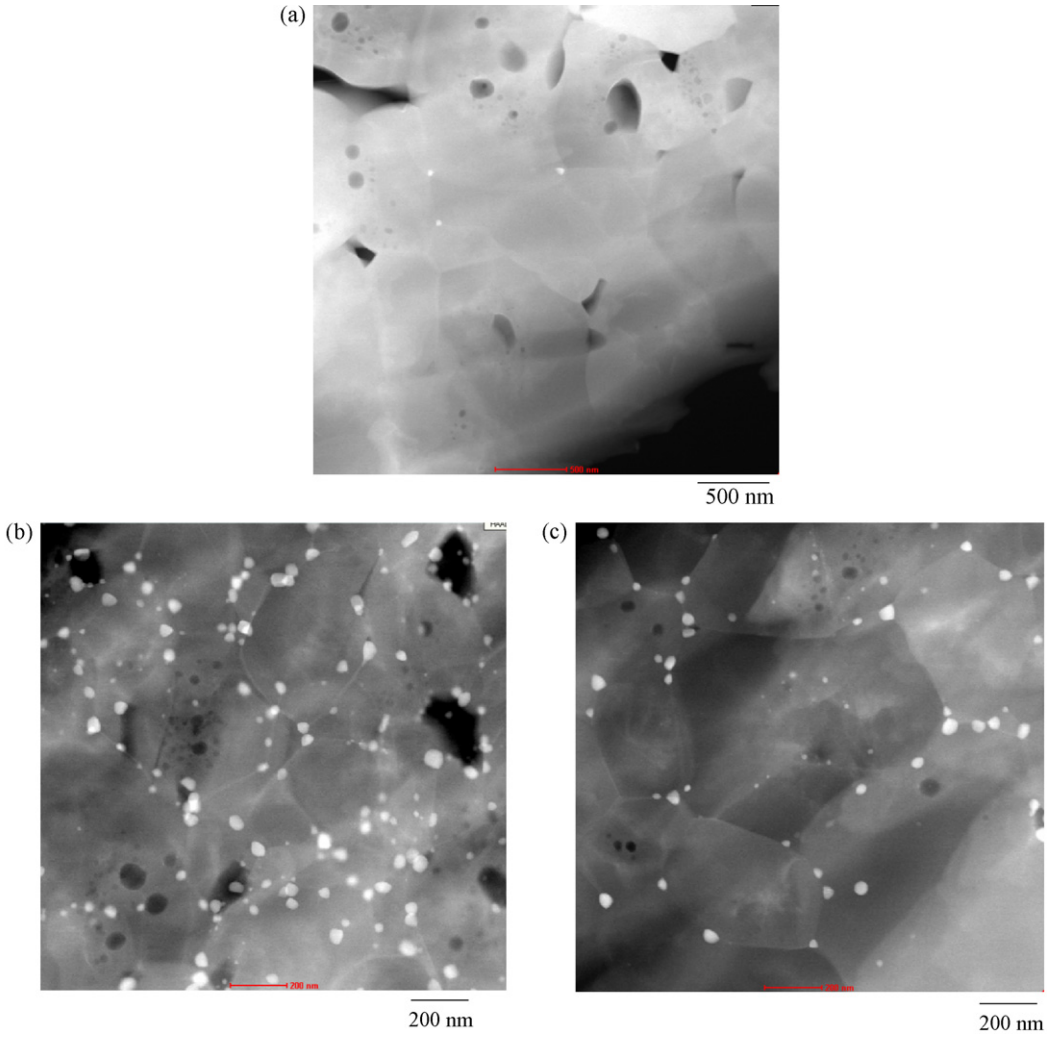

Fig. 7. HAADF STEM micrographs of samples: (a) sample 1, (b) sample 2 and (c) sample 3.

solid solution and thus the Al_2O_3 peaks shifted to lower angles in the XRD pattern. Furthermore, the color of the pieces is dark red,[29] as observed in sample 1, due to the $(Al,Cr)_2O_3$ solid solution reaction product.

Secondly, a comparison with the peaks of ALO reveals that the Al_2O_3 diffraction peaks of sample 2, as shown in Fig. 6(c), shift to lower angles, occurring simultaneously with the peaks of Cr_3C_2. Consequently, besides forming a solid solution, some of the Cr_2O_3 reacts with carbon as Eq. (1) to form chromium carbide Cr_3C_2 when the powders have been pre-sintered at 1150 °C.

Thirdly, Fig. 6(d) shows the XRD patterns of sample 3. Similar to the results of sample 2, in addition to forming a solid solution, some of the Cr_2O_3 was also carbonized. However, it transformed into mixed phases of Cr_3C_2 and Cr_7C_3 when the fluidized powders were hot pressed at 1400 °C. Berger et al.[30] reports that Cr_7C_3 is formed at an elevated temperature (>1150 °C). Moreover, the TG/DTA results of our previous paper[22] also indicate that the generation temperature of Cr_7C_3 is about 1170 °C. This carbothermal reaction process[11] can be shown as reaction (2). Consequently, not only Cr_3C_2, but also Cr_7C_3 is formed in sample 3, hot pressed at 1400 °C.

$$Cr_2O_{3(s)} + 27/7C_{(s)} \rightarrow 2/7Cr_7C_{3(s)} + 3CO_{(g)} \quad (2)$$

3.4. Microstructure of hot-pressed samples

According to Bondioli et al.[31], at temperatures of over 1000 °C the complete ranges of substitutional solid solutions are obtained. Fig. 7(a) is the HAADF STEM image of sample 1, showing almost all the Cr^{3+} replaced the Al^{3+} and formed a Al_2O_3–Cr_2O_3 solid solution.

Fig. 7(b) and (c) are the HAADF STEM images of samples 2 and 3, respectively, showing that in addition to forming a solid solution, nanosized chromium carbide particles also disperse uniformly in the alumina matrix. Comparing the HAADF STEM images of samples, sample 2 has smaller alumina grain size than others (sample 1: 1.5 μm, sample 2: 0.7 μm, sample 3: 0.9 μm.) This is because it has much nanosized particles on the Al_2O_3 grain boundaries, which effectively inhibit the grain growth. The volume percentages of the reinforced particles showing in Fig. 7(b) and (c) are 4.5 and 1.5 vol%, respectively. Conversely,

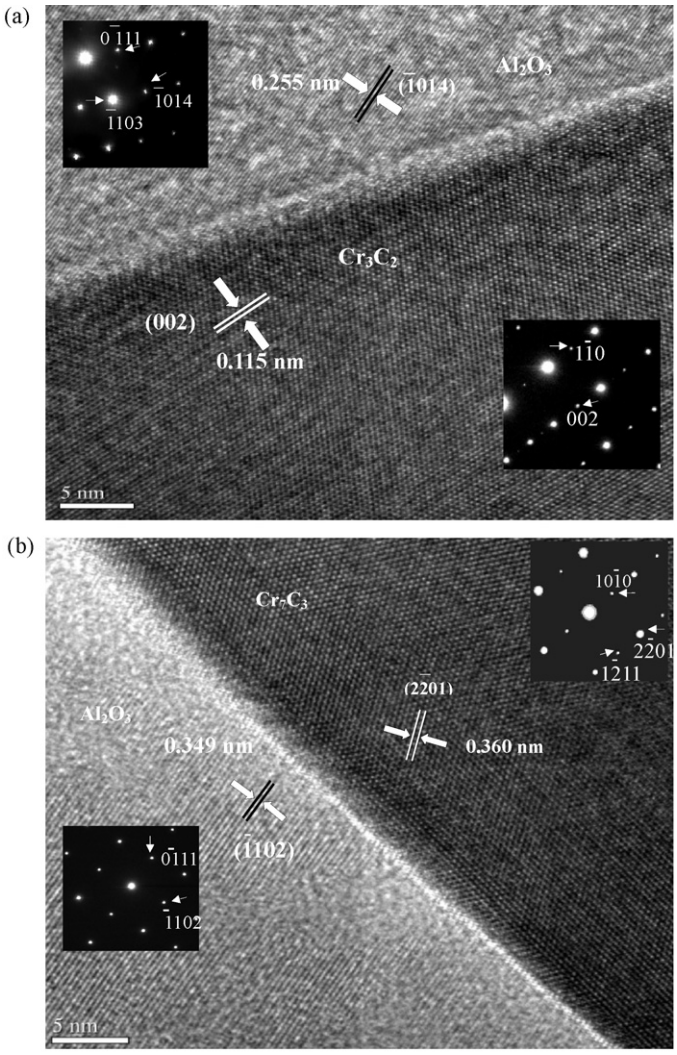

Fig. 8. Lattice images of the interfaces (a) between Cr_3C_2 and Al_2O_3, and (b) between Cr_7C_3 and Al_2O_3.

the Al_2O_3 grains of sample 1 have a larger growth size as a result of the diffusion of Cr atoms inducing grain boundary migration (DIGM).[32] The drive force for the migration is believed to rise from the coherency strain in the Cr_2O_3 diffusion zone in front of the migrating grain boundaries.

There are two HRTEM micrographs of interfaces shown in Fig. 8. One is the interface between the Cr_3C_2 and Al_2O_3 and the other is the interface between Cr_7C_3 and Al_2O_3. The interface between Al_2O_3 and Cr_3C_2 is non-coherent, as shown in Fig. 8(a). The smaller illustrations in Fig. 8(a) show Al_2O_3 with hexagonal and Cr_3C_2 with orthorhombic structure. The lattice spacing of the Al_2O_3 ($\bar{1}$ 0 1 4) is 0.255 nm and that of the Cr_3C_2 (0 0 2) is 0.115 nm. The spacing difference between these two planes is large. However, the interface between Al_2O_3 and Cr_7C_3 is semi-coherent, as shown in Fig. 8(b). Structures of both Al_2O_3 and Cr_7C_3 are hexagonal. The lattice spacing of the Al_2O_3 plane ($\bar{1}$ 1 0 2) and Cr_7C_3 plane (2 $\bar{2}$ 0 1) are 0.349 and 0.360 nm, respectively. There is little difference between the lattice spacing of these two hexagonal planes.

4. Conclusions

The method used in this study, which combines MOCVD and a fluidized bed, can fabricate nanocomposite particles in which the nanosized Cr-species are deposited uniformly on alumina particles. Cr_2O_3 reacts with free carbon and carbonizes into Cr_3C_2 at 1150 °C in vacuum condition. Solid solution of Al_2O_3–Cr_2O_3 was formed when the sintering condition was pre-sintering at 1000 °C before hot-pressing at 1400 °C. When pre-sintering at 1150 °C before hot-pressing at 1400 °C, both a solid solution of Al_2O_3–Cr_2O_3 and a Cr_3C_2–Al_2O_3 nanocomposite were formed. However, the second phase particles became a mixed phase of Cr_7C_3 and Cr_3C_2 when directly hot pressed at 1400 °C. Interface between Al_2O_3 and Cr_7C_3 is semi-coherent, while between Al_2O_3 and Cr_3C_2 is non-coherent.

Acknowledgment

The authors would like to thank National Science Council of the Republic of China for its financial support under the Contract No. NSC-92-2216-E-006-011.

References

1. Lio, S., Watanabe, M., Matsubara, M. and Matsuo, Y., Mechanical properties of alumina/silicon carbide whisker composites. *J. Am. Ceram. Soc.*, 1989, **72**(10), 1880–1884.
2. Tseng, W. J. and Funkenbusch:, P. D., Microstructure and densification of pressureless-sintered Al_2O_3/Si_3N_4. *J. Am. Ceram. Soc.*, 1992, **75**(5), 1171–1175.
3. Chou, Y. S. and Green, D. J., Silicon carbide platelet/alumina composites. I. Effect of forming technique on platelet orientation. *J. Am. Ceram. Soc.*, 1992, **75**(12), 3346–3352.
4. Huang, J. L., Lin, H. D., Jeng, C. A. and Lii, D. F., Crack growth resistance of Cr_3C_2/Al_2O_3 composites. *Mater. Sci. Eng. A*, 2000, **279**, 81–86.
5. Huang, J. L., Twu, K. C., Lii, D. F. and Li, A. K., Investigation of Al_2O_3/Cr_3C_2 composites prepared by pressureless sintering (part 2). *Mater. Chem. Phys.*, 1997, **51**, 211–215.
6. Lii, D. F., Huang, J. L., Huang, J. H. and Lu, H. H. J., The interfacial reaction in Cr_3C_2/Al_2O_3 composites. *J. Mater. Res.*, 1999, **14**, 817–823.
7. Fu, C. T., Wu, J. M. and Li, A. K., Microstructure and mechanical properties of Cr_3C_2 particulate reinforced Al_2O_3 matrix composites. *J. Mater. Sci.*, 1994, **29**, 2671–2677.
8. Fu, C. T., Li, A. K. and Wu, J. M., The effects of oxidation of Cr_3C_2 particle reinforced Al_2O_3 composites on microstructure and mechanical properties. *J. Mater. Sci.*, 1993, **28**, 6285–6294.
9. Edmund K. Storms, *The Refractory Carbides*. New York and London, 1967, p. 102.
10. Shu, K. M., Fu, C. T. and Wu, J. M., Electrodischarge-machining of Al_2O_3/Cr_3C_2 composites. *J. Mater. Sci. Lett.*, 1994, **13**, 1146–1148.
11. Bradt, R. C., Cr_2O_3 solid solution hardening of Al_2O_3. *J. Am. Ceram. Soc.*, 1967, **50**, 54–55.
12. Chate, B. B., Smith, W. C., Kim, C. H., Hasselman, D. P. H. and Kane, G. E., Effect of chromia alloying on machining performance of alumina ceramic cutting tools. *Am. Ceram. Soc. Bull.*, 1975, **54**, 210–215.
13. Davies, T. J., Emblem, H. G., Harabi, A., Nwobodo, C. S., Ogwu, A. A. and Tsantzlaou:, V., Characterisation and properties of alumina-chrome refratories. *Br. Ceram. Trans.*, 1992, **91**, 71–76.
14. Harabi, A. and Davies, T. J., Mechanical properties of sintered alumina-chromia refractories. *Br. Ceram. Trans.*, 1995, **94**, 79–84.
15. Niihara, K., New design concept of structural ceramics–ceramic nanocomposites. *J. Ceram. Soc. Jpn.*, 1991, **99**(10), 974–982.

16. Pugar, E. A. and Morgan:, P. E. D., Coupled grain growth effects in Al_2O_3/10 vol% ZrO_2. *J. Am. Ceram. Soc.*, 1986, **69**(6), C120–C123.
17. Morooka, S., Kobata, A. and Kusakabe:, K., Rate analysis of composite ceramic particles production by CVD reactions in a fluidized bed. *AICHE Symp. Ser.*, 1991, **87**, 32–37.
18. Tsugeki, K., Kato, T., Koyanagi, Y., Kusakabe, K. and Morooka, S., Electronductivity of sintered bodies of α-Al_2O_3–TiN composite prepared by CVD reaction in a fluidized bed. *J. Mater. Sci.*, 1993, **28**, 3168–3172.
19. Hua, B. and Li:, C., Production and characterization of nanocrystalline SnO_2 films on Al_2O_3 agglomerates by CVD in a fluidized bed. *Mat. Chem. Phys.*, 1999, **59**, 130–135.
20. Daizo Kunii and Octave Levenspiel, *Fluidization Engineering*. Huntington, NY, 1977, pp. 195–223.
21. Lander, J. J. and Germer:, L. H., Plating molybdenum, tungsten, and chromium by thermal decomposition of their carbonyls. *Am. Inst. Min. Metal. Eng. Tech.*, 1947, **14**(6), 1–42.
22. Lin, H. T., Huang, J. L., Lo, W. T. and Wei, W. C. J., Investigation on carbonizing behaviors of nanometer-sized Cr_2O_3 particles dispersed on alumina particles by MOCVD in fluidized bed. *J. Mat. Res.*, 2005, **20**, 2154–2160.
23. Wagner, C. D., Riggs, W. M., Davis, L. E. and Moulder, J. F., *Handbook of X-ray Photoelectron Spectroscopy*. Perkin-Elmer, Minnesota, 1979, p. 77.
24. Kazusaka, A. and Howe, R. F., Spectroscopic characterization of alumina supported transition metal carbonyl catakysts 2. $W(CO)_6$ and $Cr(CO)_6$. *J. Mol. Catal.*, 1980, **9**, 199–207.
25. Shinn, N. D. and Madey, T. E., CO chemisorption on Cr(1 1 0): evidence for a precursor to dissociation. *J. Chem. Phys.*, 1985, **83**, 5928–5944.
26. Schuste, F. and Maury, F., Influence of organochromium precursor chemistry on the microstructure of MOCVD chromium carbide coatings. *Surf. Coat. Tech.*, 1990, **43**, 185–198.
27. Bouzy, E., Bauer-Grosse, E. and Le Caer, G., NaCl and filled Re_3B-type structures for two metastable chromium carbides. *Philos. Mag., B.*, 1993, **68**(5), 619–638.
28. Bewilogua, K., Heinitz, H.-J., Rau, B. and Schulze:, S., A chromium carbide phase with B1 structure in thin film prepared By ion plating. *Thin Solid Films*, 1988, **167**, 233–243.
29. Nassau, K., *The Physics and Chemistry of Color*. Wiley, New York, 1983, pp. 77–106.
30. Berger, L.-M., stole, S., Gruner, W. and Wetzig, K., Investigation of the carbothermal reduction process of chromium oxide by micro- and lab-scale methods. *Int. J. Refract. Met. Hard Mat.*, 2001, **19**, 109–121.
31. Bondioli, F., Ferrari, A. M., Leonelli, C. and Manfredini, T. J., Reaction mechanism in alumina/chromia(Al_2O_3–Cr_2O_3) solid solutions obtained by coprecipitation. *J. Am. Ceram. Soc.*, 2000, **83**, 2036–2040.
32. Han, S. C., Yoon, D. Y. and Brun, M. K., Migration of grain boundaries in alumina induced by chromia addition. *Acta Metall. Mater.*, 1995, **43**, 977–984.